Bioglasses: Biosignal-based Biometrics using Sensors

Miguel Almeida
miguel.almeida@ist.utl.pt

Instituto Superior Técnico, Lisboa, Portugal

December 2014

Abstract

The present work aims to design an entire electrophysiological signal (ECG, EEG and EOG) acquisition system that includes the structure in which capacitive electrodes are inserted, bioamplifiers capable of filtering and amplifying the signals, a digitization network based on the Raspberry Pi and battery-based power supplies capable of powering all the electronic circuitry, including the Raspberry Pi. From the acquired signals, it was proposed to develop a biometric system capable of pre-processing, extracting features and classify individuals, in authentication and identification settings, by using three different classifiers. The whole system described constitutes the Bioglasses. At the end of presenting and describing each individual block, several tests were conducted so that their performances may be evaluated. All the blocks reflected some degree of success with the exception of the EEG bioamplifier, due to a bad PCB design, the electrode system and structure, due to badly-designed electrodes and a rudimental glasses structure, and the EEG classifiers, due to an inadequate feature extraction. Because the electrode system did not work, it was necessary no resort to a pre-existing database in order to obtain samples of the ECG and EEG. Concerning the ECG, in a authentication context, the three classifiers achieved EERs below 3%, while in the identification test, all the successful identification rates were higher than 98%.

Keywords: Bioglasses, capacitive sensors, bioamplifiers, Raspberry Pi, authentication, identification.

1. Introduction

The electrocardiogram (ECG) is arguably the most recognizable electrophysiological signal. It's obtained at the end of an electrocardiography procedure and is the name given to the recording of the electrical manifestation over time of the contractile activity of the heart. In clinical practice, the ECG is measured using the 12-derivation system, using six leads and six limb leads. The ECG has shown promise as a biometric modality. Every person exhibits the signal and contains enough information to be able to distinguish between individuals. In the last years, several studies have shown that the ECG can be acquired at different locations other than around the heart and still be usable in biometric applications[1,2].

Using surface electrodes at the scalp level, one can measure the cortical potentials that are generated due to excitatory and inhibitory post-synaptic potential developed by cell bodies and dendrites of pyramidal neurons. Physiological control processes, thought processes and external stimuli all generate signals that flow through the exceedingly large number of existing neurons, with each contributing to the overall scalp electroencephalogram (EEG). Like the ECG, the EEG has been studied as a biometric modality with some degree of success. Although the EEG's universality and uniqueness are already well-established[3–5], the setup time for an acquisition still poses some bars on the EEG's usefulness in biometric settings. [6–8] have all conducted studies towards reducing the number of electrodes necessary of an acquisition.

The electrooculogram (EOG) is derived from the Corneo-Retinal Potential (CRP) and the electric field it produces when the eye moves within its socket. By placing electrodes above, below and at the canthi of the eye it's possible to capture this field and track the position of the eye based on it. The EOG has been mainly used in a Human-Computer Interfaces (HCI) context and it has been shown that it does contain some distinguishable features, although not being very reliable. However, it can still be fused with other modalities to increase a system's performance[9].

2. The Biopotential Amplifier

A biopotential amplifier, or bioamplifier, must be able to adequately amplify the signal of interest and filter out undesired interference without causing harm to the user. The proposed bioamplifier for each signal includes an instrumentation amplifier, a 4th order low-pass Butterworth filter, a 2nd order high-pass filter based on a differential approach and an active twin-T notch filter. A diagram of the filter portion of the bioamplifier is shown

In order to evaluate the performance of the circuits before ordering the printed circuit boards (PCB), they were tested in terms of bandwidth, gain, Signal-to-Noise and Distortion Ratio (SINAD) and noise quantization. No test revealed any major problem but the upper cutoff frequency of the EEG channel was reduced in order to facilitate the use of the Independent Component Analysis (ICA) algorithm in the digital processing stage.

The sensor capacitance developed between the skin and the copper foil electrode is akin to that of parallel-plate capacitor and thus it is given by:

$$C_{sensor} = \varepsilon_0 \varepsilon_r \frac{A}{d}$$

where $\varepsilon_0 = 8.85 * 10^{-12} F \cdot m^{-1}$ is the dielectric constant, ε_r is the relative dielectric constant of the insulating material, A is the area that overlaps both surfaces that overlaps and d is the distance between them. Due to the variability of parameters ε_r and d, it's not possible to give an exact figure However, this value should be kept as high as possible. This is due to the generation of an RC network with the instrumentation amplifier's input impedance and the bias resistors placed at its inputs that imposes an high-pass characteristic with passband gain:

$$G = \frac{C_{sensor}}{C_{sensor} + C_{in}}$$

and cutoff frequency:

$$\omega_0 = \frac{1}{R_{bias}(C_{sensor} + C_{in})}$$

where R_{bias} is the resistance of the bias resistor and C_{in} is the input capacitance of the instrumentation amplifier. If sensor capacitance is not kept large, the gain becomes too small and the signal is severely attenuated and the cutoff frequency also tends to higher frequency regions. Setting a large bias resistor also helps in keeping the cutoff frequency small. However, this value must be very large. In a conducted experiment, even when using electrodes with a larger area than the ones placed in the glasses, the cutoff frequency developed by the RC network still reached $41.3Hz$ when setting the bias resistors with a value of $100M\Omega$.

3. Raspberry Pi

The Raspberry Pi (RPi) is a credit card-sized, single-board computer designed by the Raspberry Pi Foundation primarily as an educational tool to introduce children to the basics of computer science. It has all the common capabilities of an ordinary computer including web browsing, game playing and video watching, with the added possibility of being used in electronics projects. Besides the familiar HDMI, USB and Ethernet ports, the RPi also carries a set of low-level peripherals that are useful for connecting directly to chips and subsystem modules, like analog-to-digital converters (ADC), without having to add any new circuitry. These general purpose input/output (GPIO) pins are exclusively tolerant to $3.3V$ logic levels which means anything higher than this value has a high risk of damaging the device.

In a system that aims to acquire biological signals, it is important to design an acquisition network capable of achieving high sampling rates. Furthermore, there was a need to ensure that the signals all exhibited some high level of time coherence (same time instant samples between channels should only have a double digit microsecond delay between them). With the RPi, in its default state, obtaining such short conversion periods is hugely limited by the long latencies of the Linux kernel. In order to turn the kernel more real-time friendly, it was patched with the PREEMPT_RT patch[10]. Several

aspects still needed to be adjusted, both at the kernel and at the script level, in order to optimize the overall real-time performance and while the script-related changes are discussed later, the ones concerning the kernel itself are presented: overclocking the CPU, using a specialized of high-resolution timers, altering the CPU power management and allocating more RAM to the CPU from the Graphics Processing Unit[10].

The acquisition algorithm is composed of two different programs: one written in Python and one written in C. While the actual acquisition code runs in the latter, the Python code interfaces with the user and sends the acquired data to a host computer. The C script can be divided into three different stages:

- Real-time initialization and memory locking: the script presents itself to the kernel as a high-priority, real-time task.
- GPIO and Serial Peripheral Interface (SPI) initialization: this block of functions initiates the GPIO and SPI interfaces.
- Acquisition cycle: the block of code where the samples are acquired from the ADC and stored by the RPi. When the acquisition ends, the samples are stored into a .txt file and set to a host computer.

4. Power Supply

Two independent battery-based power supplies were considered, one focusing on the bioamplifiers while the other on the RPi. Ultimately, using two different supplies meant finding a regulator that could maintain high efficiency when outputting both small and large currents. Both the RPi and all of the integrated components (IC) chosen for the PCBs are capable of operating at $5V$ and thus, the main demand on the power supplies was that they should produce a steady $5V$ at their output.

The first supply system powers the bioamplifier boards, which contains the operational and instrumentation amplifiers. Consulting the corresponding datasheets reveals that the maximum current drain for the entire system amounts to $26.1mA$. The second supply powers the remaining components which are the Raspberry Pi model A, the ADC and the multiplexer. Because it was not enough to consult the datasheets of the RPi to know the current demands, a test was performed on order to get an idea of the values involved. The maximum current drain observed was $303mA$. A boost switching regulator was considered for the supply boards. Due to some unbalanced voltage supply issues and a short linear input range of the instrumentation amplifier, , the board powering the RPi uses two $1.5V$ cells and the one that powers the bioamplifiers uses three.

5. PCBs

Three PCBs were soldered: the ones with the bioamplifiers, the ones destined for the power supplies and another with the ADC and multiplexer responsible for digitizing the signals and sending them to the RPi.

Regarding the bioamplifier boards, an INA121 was chosen among other instrumentation amplifiers due to its low supply voltage (as low as $V_S = \pm 2.25V$) and its low power consumption (typically $0.450mA$), being optimal for battery operated systems. Other important characteristics worth mentioning are the $106dB$ CMRR when the gain is 10, and the $4pA$ bias current[11]. Concerning the operational amplifiers, the LMC7101 was chosen, not only for its advantageous power ratings, but also for its overall specifications[12]. The gain of the instrumentation amplifier is regulated by a 3223W-1-504, an SMD potentiometer with a $500k\Omega$ track resistance,

The board containing the ADC and multiplexer is henceforth referred to as the conversion board. When searching for a suitable multiplexer, the best one found was the ADG708, a $18ns$ switching time, 8Ω on-resistance multiplexer capable of operating from a $3{,}3V$ single supply with a maximum current drain of $1\mu A$[13]. Similarly, the ADC that represented the best compromise was the AD7680: despite being relatively price accessible, it offers a $100kSPS$ sampling rate and a $16bit$ resolution while only draining a maximum of $2.8mA$ at $3.3V$[14].

For the supply boards, the boost device chosen was the LT1302-5. This package excels due to its high efficiency over a wide range of output current, going as far as being able to output $600mA$ at $5V$ from an input supply as low as $2V$[15]. Particular attention was given when designing this board. If high current functions

were allowed to run next to the control functions, then the devices would not work as expected.

Each board was submitted to a battery of tests. For the power supplies, the tests tried to evaluate their stability and efficiency, with the first being a qualitative test and the second a quantitative one. Figure 1 shows the output voltage transition of the RPi supply board from no load to a load of 100Ω. In Figure 2, the plot for the efficiency of the same power supply is illustrated.

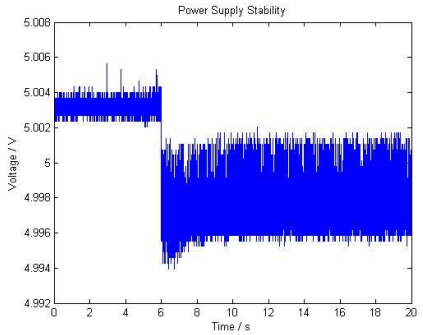

Figure 1 - Transient response of the RPi supply board when a 100Ω is placed at is output, when there was no load previously.

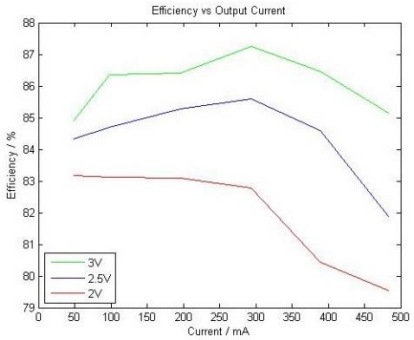

Figure 2 - Efficiency curves concerning the board that power the RPi.

For the bioamplifier boards, the same tests were done as in the breadboards but here the gain and sweep tests were grouped into one. Figures 3-6 depict a comparison between plots of the real and ideal magnitude transmissions for each channel. Tables 1 and 2 gather the results for the SINAD and noise tests, respectively.

The conversion board was tested in conjunction with the RPi since the RPi provides the clock signal and the address lines for the ADC and multiplexer, respectively. Because it was unknown what kind of conversion and frequency periods the whole system was capable of achieving, a test was performed to verify what that limit was. The measure that evaluated the performance was the Effective Number of Bits (ENOB). The largest obtained value was 8.25 for a sampling frequency of $100Hz$ and a conversion frequency of $2500Hz$. For these values, the values of the SINAD and Signal-to-Noise Ratio (SNR) were $51.43dB$ and $52.37dB$, respectively. Also, for this particular ENOB value, the real measured frequency amounted to: $99.9871 \pm 0.1390Hz$.

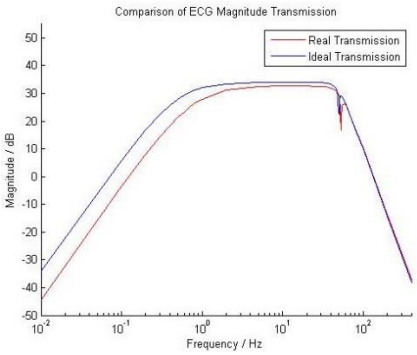

Figure 3 - Comparison between the ideal and real transmissions calculated obtained for the ECG.

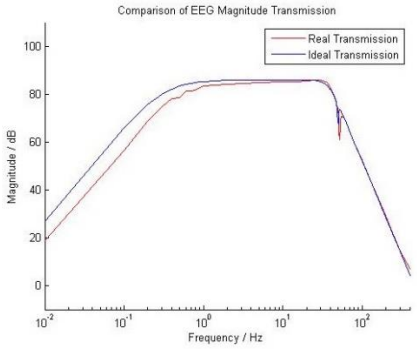

Figure 4 - Comparison between the ideal and real transmissions calculated obtained for the EEG.

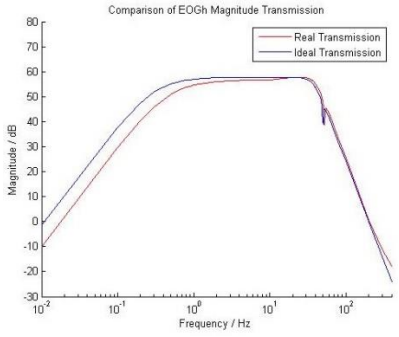

Figure 5 - Comparison between the ideal and real transmissions calculated obtained for the EOGh.

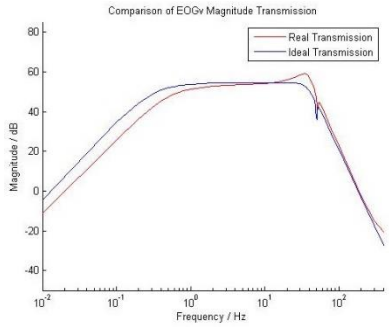

Figure 6 - Comparison between the ideal and real transmissions calculated obtained for the EOGv.

Table 1 - SINAD values obtained for each channel at each specific frequency.

	Frequency (Hz)			
	2	**10**	**30**	**70**
ECG SINAD (dB)	58.89	46.74	44.84	49.72
EEG SINAD (dB)	11.00	10.61	11.26	−8.20
EOGh SINAD (dB)	44.35	40.68	41.80	26.42
EOGv SINAD (dB)	45.19	43.68	46.77	27.89

Table 2 - Noise parameters obtained for each channel.

	Mean Value (mV)	**RMS value (mV)**	**Power (mV^2)**	**Most represented frequency (Hz)**
ECG	29.43	29.44	866.70	1
EEG	$-1.11 \cdot 10^3$	$1.11 \cdot 10^3$	$1.24 \cdot 10^6$	50
EOGh	191.88	191.89	$36.82 \cdot 10^3$	50
EOGv	16.42	16.50	272.31	1

6. Bioglasses

With the aim of capturing the ECG, EEG and EOG electrophysiological signals, some sort of hardware was needed to place the capacitive electrodes. Excluding the ECG, which is traditionally captured as close to the heart as possible, the remaining signals are all acquired at different locations in the skull. However, research showed that some work has been done where neckbands are utilized to measure the ECG[16,17]. With all the signals thus concentrated around the head/neck region, a helmet or a pair of glasses were the ideas that naturally followed, with the latter being the one chosen in the end.

The traditional framework of a pair of glasses is enough to place the EOG signals if the rims are designed with sufficient thickness, but it isn't enough for the remaining physiological signals. Two extensions were added to the traditional eyeglasses' design: first, the temples that usually terminate slightly behind the ear are prolonged and united at the back of the head as close as possible to the Oz position in the 10-20 electrode placement system; second, right before the temples pass the ear, a prolongation was added that continues downward towards the side of the neck and this is where the electrodes are placed to capture the ECG. An extra electrode is placed between the lenses and all along the inner rim, all regions that are in contact with the nasal bone, in order to obtain the body reference potential. Figure 7 shows the placement of the electrodes in the 2D schematic.

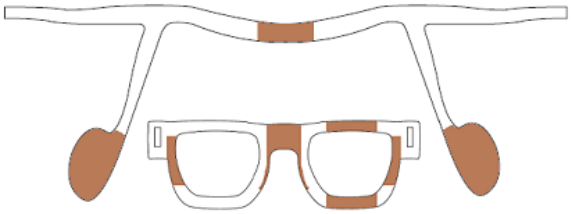

Figure 7 - 2D design of the glasses structure. The brown areas coincide with the location of the electrodes.

Each electrode has a wire stemming from it that is connected to the corresponding bioamplifiers. For organization sake and to make it easy to handle the hardware, the wires are all bundled together by duct tape before reaching the PCBs. Due to their close proximity along a relatively long distance, some measures were taken in order to minimize the effects of crosstalk through capacitive coupling. All the wires were individually wrapped with aluminum foil connected to the body reference potential, providing proper shielding against electrical interference. Wires carrying signals that belong to the same bipolar channel, e.g. the ECG and the EOGs, were also twisted together to further reduce electromagnetic interference.

In the final test to acquire the signals using the developed structure, the bioamplifiers, the conversion board, the RPI and the power supplies, no discernible physiological signals could be observed, noise and motion artifacts were the only components present. In the EEG, only saturation of the upper voltage rail was

observerd. The source of the issue were the sensor electrodes themselves. Using contact electrodes and connecting the bioamplifiers to a NI BNC-2110 acquisition board was enough to observe the signals. The plots shown in Figures 8-11 illustrate the various signals after filtering (except the EEG that is shown raw).

7. Biometrics

Since no signal database was created, the one provided by the HiMotion research project[18] was used. The project aimed to capture the ECG and EEG, among other signals, from 27 subjects that were undergoing tests in a computer. For this work, only the concentration tests were considered. The ECG was measured at the fourth intercostal space in the midclavicular line and the EEG was recorded at the Fp1, Fp2, Fz and Oz locations in the 10-20 system.

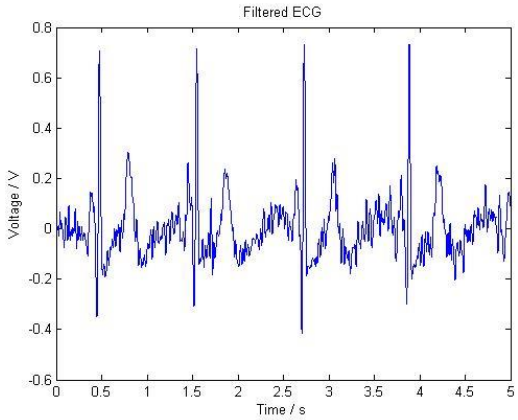

Figure 8 – Filtered ECG signal acquired using contact electrodes in the neck.

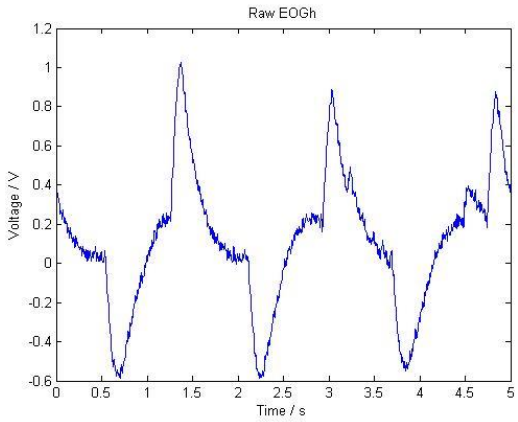

Figure 9 -Filtered EOGh (left gaze) signal acquired using contact electrodes.

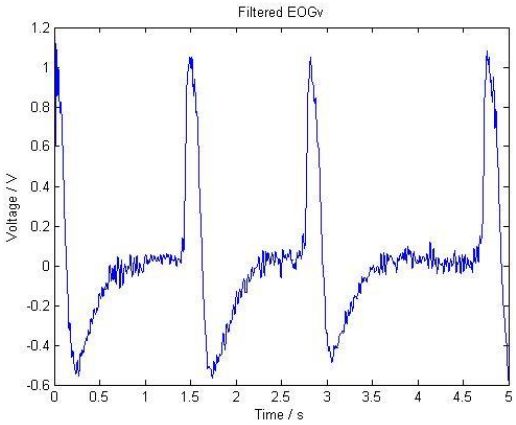

Figure 10 - Filtered EOGv (eye blink) signal acquired using contact electrodes.

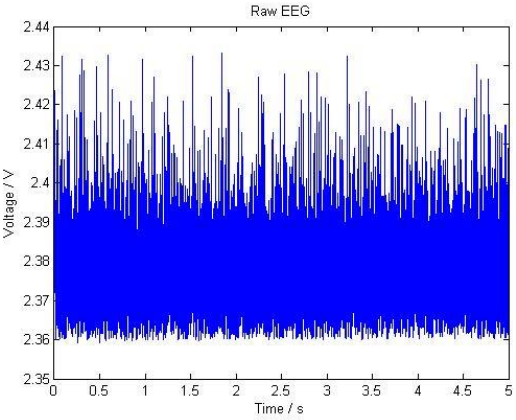

Figure 11- EEG signal acquired using contact electrodes. Only saturation of the positive rail can be observer.

In the case of the ECG, the signal was pre-processed in order to find the locations of the R peak. Then, the features extracted consisted in all of the samples found 0.2 before and 0.4 seconds after these peaks. 150 randomly selected heartbeats were extracted per subject, 50 of which were used for training and the remaining for testing. For the EEG, each set of features contained the beta band power differences between consecutive 5 second segments from each individual channel. For each subject, 80 feature sets were randomly selected, a third of which was selected to train the classifier and the rest to test it.

In order to classify the templates, three distinct classifiers were used: k-NN based on the Euclidean distance ($k = 3$), k-NN based on the Cosine distance ($k = 3$) and SVM. The performance for each classifier

was evaluated for the two different biometric settings, authentication and identification. Each performance test was run fifty times in order to be statistically meaningful. In the authentication test, the classifiers were given several different-valued thresholds, ranging from 0 to 100 in steps of 1. The classifiers were evaluated in terms of False Rejection Rate (FRR), or its complement the True Rejection Rate (TAR), the False Acceptance Rate (FAR) and the Equal Error Rate (EER). However, these parameters are only useful to compare the system itself, not to compare different systems. For that, the Receiver Operating Curves (ROC) were plotted. The results for all the classifiers are all illustrated in Figures 12-19. For the identification test, the classifiers were evaluated on their ability to correctly identify the individual presenting itself to the system. Table 3 shows the identification success rate for each classifier and each biosignal.

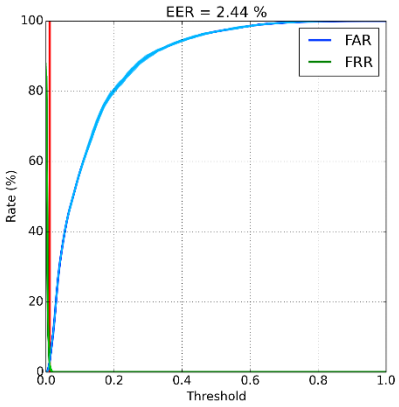

Figure 12 – Graphic plotting the FAR and FRR curves against each threshold for the ECG Cosine k-NN. The corresponding EER is also shown.

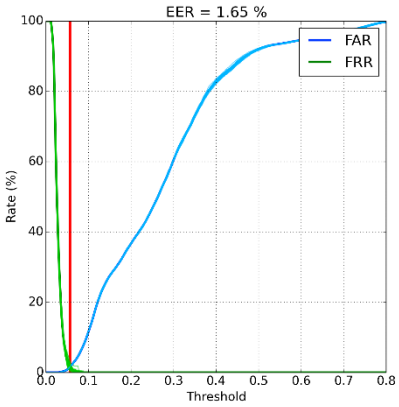

Figure 13- Graphic plotting the FAR and FRR curves against each threshold for the ECG Euclidean k-NN. The corresponding EER is also shown.

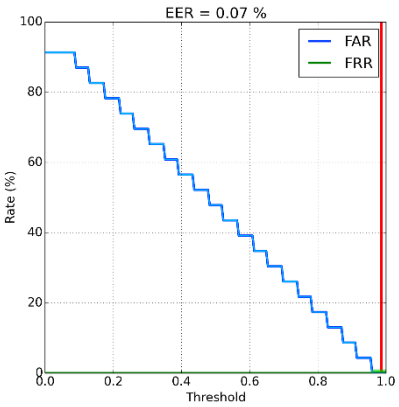

Figure 14 - Graphic plotting the FAR and FRR curves against each threshold for the ECG SVM. The corresponding EER is also shown.

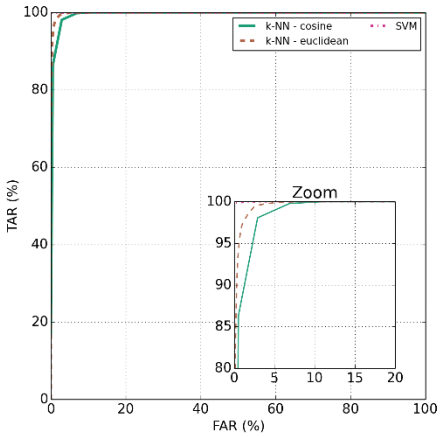

Figure 15 - ROC curves for the ECG classifiers.

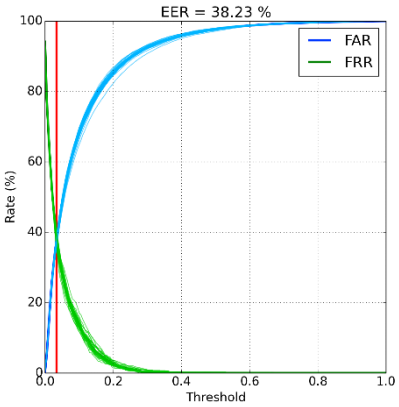

Figure 16 - Graphic plotting the FAR and FRR curves against each threshold for the EEG Cosine k-NN. The corresponding EER is also shown.

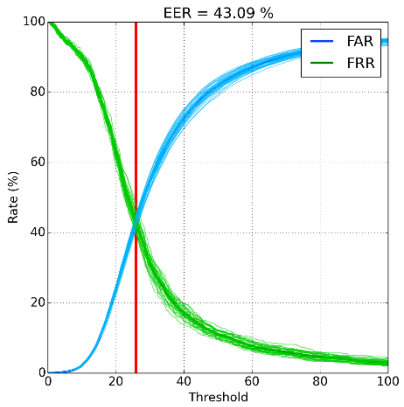

Figure 17 - Graphic plotting the FAR and FRR curves against each threshold for the EEG Euclidean k-NN. The corresponding EER is also shown.

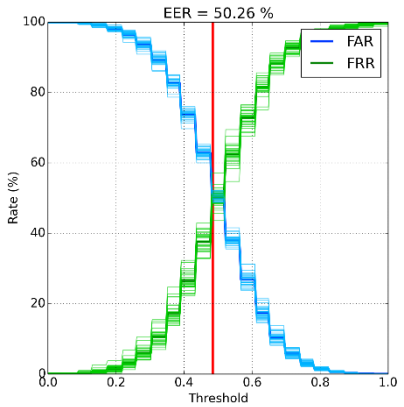

Figure 18 - Graphic plotting the FAR and FRR curves against each threshold for the ECG SVM. The corresponding EER is also shown.

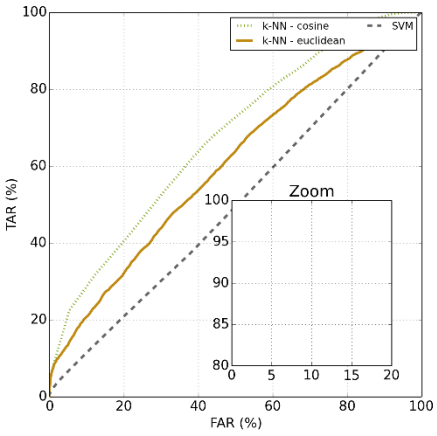

Figure 19 - ROC curves for the EEG classifiers.

Table 3 - table containing the success classification rates for the identification setting

	Euclidean distance-based k-NN (%)	Cosine distance-based k-NN (%)	SVM (%)
ECG	100	98.70	99.86
EEG	17.72	26.08	5.37

8. Discussion

The largest noise parameters exhibited in Table 2 are clearly the EOGh and EEG, particular the latter. This can be explained in two different ways: the first is related to the notch filter not being really centered on the $50Hz$ noise component. Although it's not very clear from the graphic of Figure 5 due to the logarithmic scale of the x-axis, some displacement is noticeable between the ideal characteristic and the real one at this particular frequency. This is mainly due to the small dispersions of the SMD components on the PCBs. Due to the difficulty of achieving such a fine tuning in an analog circuit, there are two possible alternatives: either implement a notch with a smaller quality factor and, consequently, wider bandwidth around the central frequency, or implement the filter digitally, provided certain measures are taken in order to minimize noise, like resorting to shielding and twisted pair cabling. The second reason, and probably the main reason why the EEG exhibited such poor results, is related to inexperience when first designing the PCBs. It could also be attributed to a mistake due to bad soldering but considering that the tests were conducted on a second version of the board (an extra board with the same design was provided by the PCB manufacturer) and that the first version exhibited the exact same problems, the problem is most likely within the design itself.

In Table 1, although the SINAD values aren't bad, excluding the EEG for now, they are still low for a bioamplifier. In case of the EEG, such bad results clearly corroborate the previous statement of some defect in board, in design or in both. For the remaining three channels, the introduction of the instrumentation amplifier and the bias resistors are a source of SINAD degradation, especially considering the high values involved ($10G\Omega$). As it was mentioned in Section 2, when

one manually sets the bias resistors, it's important to ensure that the resistors are closely matched so as not to decrease the CMRR. However, the bias resistors used in this work were rated as having a dispersion of $\pm 25\%$[19] which is exceedingly high. If common-mode signals are allowed to creep in large proportion into the circuit then the overall SINAD is sure to decrease. In order to increase the SINAD values, besides acquiring bias resistors with less dispersion, possible workarounds could be dropping the notch filter and use a digital filter, or using a high-pass filter that isn't based on a differential design, which can also introduce unwanted signal components if the passive components are not properly tuned.

Overall, the filters' real magnitude transmission was very close to the ideal one. Across all channels, the high-pass filter seems to be a slightly skewed but this is only due to the dispersion in the values of the capacitor. The only filter that deserves particular attention is the one that concerns the EOGv channel. The "knee" right before the magnitude starts rolling off to higher frequencies is a clear consequence of the dependency of the quality factor of the Butterworth filter on the gain.

The acquisition block that obtained the poorer results was the conversion system: ADC, multiplexer and RPi. Obtaining such a low ENOB for all frequency combinations when the proposed ADC is $16bit$ is not acceptable. However, the problem does not reside in the conversion board but in the RPi itself. Despite all the efforts and changes to the firmware, the RPi is not reliable when tasks are expected to occur within such short time periods. The problem is not related to the RPi not being able to meet these time requirements because it is capable of doing so. The issue is that the system cannot meet these requirements consistently. [20] conducted an independent study on a PREMPT_RT-patched Linux kernel to verify what sort of latencies can still be expected. Even on a system with a faster processor than the RPi, the latency that guaranteed a task to be performed 100% of the time was around $800\mu s$. By itself, this value is not that bad but considering that the median value for the measured latencies was $99\mu s$, it's obvious that a reasonable fixed value for the latency can't be expected or, in other words, it becomes apparent that the system is not deterministic. This is the reason why the acquisition system exhibits such a skewed sampling frequency and a high jitter. A system solely dedicated to signal acquisition and digitization needs to be employed instead of the RPi.

Concerning the constructed eyewear, there may have been several sources for why the system failed. In the case of the EEG, despite the corresponding channel not working properly, it was always a difficult signal to acquire due to their very small nature and due to hair, which carries some level of static electricity. However, the EOGh and the ECG were amenable to be obtained. During the test stage, the glasses were firmly secured to the head so that even if the subject moved his head, the glasses would move accordingly. Even so, because the glasses are handmade and are still in a very early stage of conception, there is a great deal of motion artifacts. Also, for the same reason, minute differences in the area of the electrodes or the distance to the skin between signals belonging to the same channel may have also been a strong reason as to why the system failed.

The classification results of the EEG and ECG were polar opposites of one another. Every classifier exhibited strong performances when dealing with the ECG, both in authentication and identification settings. However, despite the high classification rates, the proposed feature set, a complete heartbeat, puts some strain on the computer due to the large size of the set, particularly in the training stage. It should be noted that although the classifiers were evaluated using ECG from a different database, the ECG captured at the neck as seen in Figure 8 shows potential to be used in a biometric application. At the other end of the spectrum are the classifiers' performances for the EEG signal. Theoretically, the performances shouldn't have been so bad. The beta rhythm is usually acquired from a subject in the frontal region of the scalp while his mind is active and that was exactly the case in this work. There is the possibility the features extracted from the Oz channel may have degraded the performance of the remaining channels. Also, the EEG was divided into several five second segments, which was a value chosen arbitrarily and may have been too large. Finally, because no EOG signals were acquired during the HiMotion project, the

acquired EEG may have been contaminated by the eye signals.

9. Conclusion and Future Work

In this work, a system capable of acquiring signals using sensors placed in eyeglasses, and capable of performing biometric recognition based on these signals was proposed. At this moment, the glasses and the acquisition system are built separately but, in future works, the goal is to design a standalone, fully-integrated and fully-functional system.

The full system includes bioamplifiers capable of filtering and amplifying the ECG, EEG and EOG, a digitization network based on the Raspberry Pi and battery-based power supplies capable of fully powering the previous blocks. The signals were then used in a biometric context to evaluate their potential as a biometric trait. The classifiers utilized were SVM and two different distance-based k-NN algorithms. All the blocks were constructed with some degree of success with the exception of the EEG bioamplifier, due to poorly designed PCBs, the electrode system and structure, due to badly-designed electrodes and due to the rudimentary nature of the constructed eyeglasses structure, and the EEG classifiers, due to inadequate feature extraction.

For future work, a thorough study towards verifying the possibilities and limitations of sensors based on capacitive coupling, namely in terms of distance between skin and electrode, electrode area and interaction with the initial stages of the bioamplifiers is recommended. Also, design of a single board that encompasses all the bioamplifiers, ADC, multiplexer and power supply. Lastly, exclusion of the RPi from any sort of vital signal acquisition in favor of a dedicated system capable of providing a reliable clock source.

10. References

1. Israel S a., Irvine JM, Cheng A, Wiederhold MD, Wiederhold BK. ECG to identify individuals. *Pattern Recognit.* 2005;38(1):133-142. doi:10.1016/j.patcog.2004.05.014.

2. Santos M, Fred A, Silva H, Lourenço A. Eigen Heartbeats for User Identification. *6th Int. Conf. Bio-inspired Syst. Signal Process.* 2013:1-5. Available at: http://www.lx.it.pt/~afred/papers/Eigen Heartbeats for User Identification.pdf.

3. Palaniappan R, Mandic DP. EEG Based Biometric Framework for Automatic Identity Verification. *J. VLSI Signal Process. Syst. Signal Image. Video Technol.* 2007;49(2):243-250. doi:10.1007/s11265-007-0078-1.

4. Palaniappan R, Mandic DP, Member S. Biometrics from Brain Electrical Activity : A Machine Learning Approach. 2007;29(4):738-742.

5. Palaniappan R. Method of identifying individuals using VEP signals and neural network. *IEE Proc. - Sci. Meas. Technol.* 2004;151(1):16. doi:10.1049/ip-smt.

6. Gupta CN, Khan YU, Palaniappan R, Sepulveda F. Wavelet Framework for Improved Target Detection in Oddball Paradigms Using P300 and Gamma Band Analysis. *Soft Comput.* 2009;14(2):61-67.

7. Poulos M, Rangoussi M, Chrissikopoulos V, Evangelou A. PERSON IDENTIFICATION BASED ON PARAMETRIC PROCESSING OF THE EEG. (1):2-5.

8. Yang S, Deravi F. On the Effectiveness of EEG Signals as a Source of Biometric Information. *2012 Third Int. Conf. Emerg. Secur. Technol.* 2012:49-52. doi:10.1109/EST.2012.8.

9. Mordini E, Dimitros T, eds. *Second Generation Biometrics: The Ethical, Legal and Social Context*. Springer; 2012.

10. RTwiki. Available at: https://rt.wiki.kernel.org/index.php/Main_Page. Accessed November 30, 2014.

11. Systems BO. FET-Input , Low Power q GENERAL PURPOSE INSTRUMENTATION. 1998.

12. Lmc S. LMC7101 / LMC7101Q Tiny Low Power Operational Amplifier with Rail-to-Rail Input and Output. 2013;(September 1999).

13. Sheet D. Low Voltage 4- / 8-Channel Multiplexers. 2013.

14. Diagram FB, Description G, Highlights P. 16-Bit ADC in 6-Lead SOT-23. 2011.

15. Corporation LT. SYMBOL. :1-16.

16. Mizuno A, Okumura H, Okazaki H, Hitsuda T, Matsumura M. Non-Restrictive Method of ECG R Wave Measurement Using a Neckband. *IEEJ Trans. Electron. Inf. Syst.* 2008;128(11):1619-1624. doi:10.1541/ieejeiss.128.1619.

17. Ikeda S, Ishimura H, Matsumura M. Non-restrictive measurement of Pulse Transit Time using ECG Sensor and PPG Sensor mounted on the neckband . 2009:1130.

18. Gamboa H, Silva H, Fred A. HiMotion Project. 2007:1-24.

19. Data E. High Value Surface High Value Value Surface Surface Mounted Resistors Mounted Resistors Resistors Mounted. :20-21.

20. Brown JH, Martin B. How fast is fast enough ? Choosing between Xenomai and Linux for real-time applications.